

7

Systematic study of organic solar cells cross-section by EDS to correlate donor-acceptor vertical concentration gradients and device performances

Varun VOHRA^{1*}, Nur Tahirah Razali² and Hideyuki Murata^{3*}

¹ Department of Engineering Science, The University of Electro-communications, Japan

² Department of Mechanical and Manufacturing Engineering, Universiti Malaysia Sarawak, Malaysia

³ School of Materials Science, Japan Advanced Institute of Science and Technology, Japan

*Corresponding authors

Outline

Introduction.....	129
Methods to generate the adequate vertical concentration gradients in P3HT:PCBM OSCs.....	131
Controlling the vertical concentration gradient with amorphous P3HT in SD-OSC active layers	131
Ideal vertical concentrations in increased polymer crystallinity SD-OSC devices.....	134
Investigating the effect of thermal annealing on P3HT:PCBM BHJ-OSC performances.....	136
Correlation between fabrication conditions, concentration gradient and device performances in high efficiency PNTz4T:PC71BM BHJ-OSC devices	140
Multilayer structures in PNTz4T:PC71BM films deposited on TiOx coated ITO substrates.....	140
Comparison between continuous vertical concentration gradients and multilayered structures in PNTz4T:PC71BM regular architecture devices.....	142
Conclusion.....	144
References.....	144

Introduction

Organic solar cells (OSCs) fabrication is an emerging technology for high-productivity manufacture of photovoltaic cells using low-cost processes.^{1,2} Compared to the commercially available state-of-the-art silicon technology, OSCs have been introduced relatively recently but their performances have been steadily increasing over the past decade with record power conversion efficiencies (*PCEs*) now approaching those of lab-scale amorphous silicon cells and dye-sensitized solar cells.³⁻⁶ Furthermore, with an increasing number of scientists studying OSCs, their working principle is now much better known compared to when researchers at Kodak first fabricated these devices.⁷ In fact, OSC devices are fabricated using a simple vertical device architecture consisting of an active layer which includes two materials, namely, the electron donor and the electron acceptor, sandwiched between two electrodes with potentially additional charge selection layers. While electron donors can be small molecules or macromolecules (conjugated polymers), the most widely studied electron acceptors belong to the fullerene family.^{8,9} Due to their processability, a particular attention has been given to the conjugated polymer systems, especially since the introduction of poly(3-hexylthiophene) (P3HT) as electron donor which resulted in *PCEs* reaching up to 6.5%.^{10,11} Over the past couple of years, the *PCEs* of OSCs have been further improved with a new generation of conjugated block copolymers such as PNTz4T, a quaterthiophene–naphthobisthiadiazole copolymer.^{3,12,13} Be it with P3HT or PNTz4T (and other low bandgap copolymers), a particular attention should be given to the morphology of the active layer as it controls the main device parameters in OSCs. For instance, the short-circuit current density (J_{sc}) highly depends not only on the size of the electron donor- and electron acceptor-rich domains but also on their relative positioning with respect to the anode and the cathode. Similarly, the donor-acceptor vertical concentration gradient, which plays a decisive role to improve the charge collection efficiency, has a major impact on the fill factor (*FF*) of the devices.^{14,15}

Some commonly used analytical techniques for OSC active layers include surface characterizations by AFM,¹⁶ photoluminescence quenching measurements,¹⁷ or defocused electron microscopy¹⁸ which either approximate the donor and acceptor domain sizes or estimate the charge generation efficiency. These characterizations only provide information on the bulk or surface properties of the thin films and they cannot be used to evaluate the donor-acceptor concentration gradients in the vertical direction (along the cross-section of the device). To do so, methods such as XPS depth profiles have been introduced, in which the thin films are characterized in a layer-by-layer manner following a surface characterization/etching step/surface characterization cycle.¹⁹ However, repetitive etching of thin layers at the surface of the films often results in degradation or morphological modification in the active layer and unreliable data. Ellipsometry and neutron reflectometry, on the other hand, provide powerful tools to characterize the active layer morphologies in both lateral and vertical directions.^{16,20} Nonetheless, these methods highly depend on the accuracy of the models used for the fittings and how well the collected data fit with these models. Additionally, they do not permit to directly visualize the concentration gradients formed within the active layer. Since 2012, we have introduced an alternative characterization technique to obtain direct visualization of the electron donor-electron acceptor vertical concentration gradient in OSC active layer by looking at the device cross-sections with scanning transmission electron microscopes (STEMs) equipped with energy-dispersive X-ray elemental mapping spectroscopy (EDS).²¹⁻²⁴

EDS, which was first applied for materials and device characterization by Fitzgerald *et al.* (1968), is a powerful and yet easy to use technique for elemental analysis.²⁵ EDS consists of detecting the characteristic X-rays produced by each element after bombarding a sample with high energy

electrons in an electron microscope. In fact, when coupled with a STEM, it becomes possible to analyze the vertical compositions of thin films with thicknesses down to 30 nm. In 2012, our pioneer study using EDS to characterize the cross-section of sequentially deposited OSCs (SD-OSCs) demonstrated the potential of this analytical technique to obtain additional information on the requirements for high efficiency SD-OSC fabrication.²¹⁻²⁴ In fact, since then, EDS has been regularly applied to high *PCE*, OSCs and perovskite solar cells characterizations.^{26,27}

Figure 7.1 displays the typical sample preparation sequence for EDS analysis where a thin slice (less than 100 nm thick) of the samples deposited on thick substrates (e.g. glass) is cut using focused ion beam and then placed lying down on the sample stage for analysis. In Figure 7.1, we display images collected for a sample in which an electron acceptor-rich layer is trapped between an approximately 30 nm thick bottom electron donor-rich layer and an approximately 10 nm thick top electron donor-rich layer. While EDS provides direct visual information on the concentration gradient obtained in these devices, other cross-section characterization techniques, such as SEM, tend to overlook the thin top layer due to lack of contrast. Note that EDS is not just an imaging technique but concentration profiles can be obtained by plotting the elemental counts against the X (or Y) position of the scan. The sample presented in Figure 7.1 corresponds to the active layer resulting from sequential deposition of a P3HT layer from chlorobenzene (CB) coated with the state-of-the-art fullerene derivative (Phenyl-C₆₁-butyric acid methyl ester, PCBM) deposited from dichloromethane (DCM) with the active layers annealed in air after metal electrode deposition.

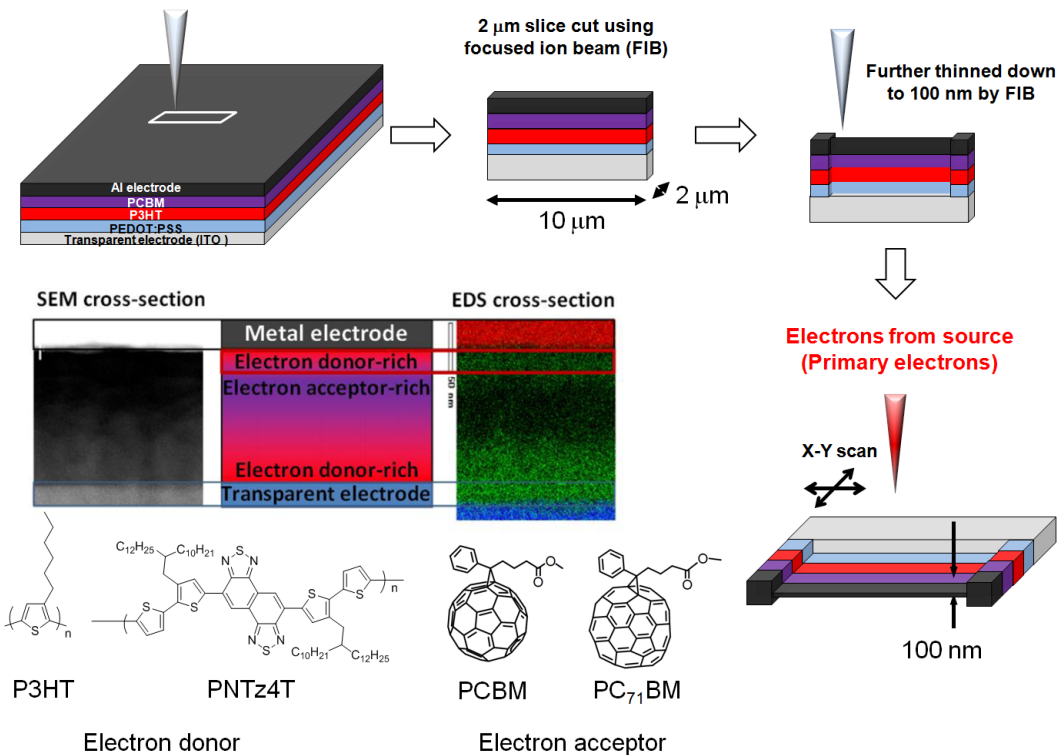


FIGURE 7.1

Schematic representation of the EDS sample preparation and comparative analysis of the same sample using SEM and EDS. Molecular structures of the electron donor and acceptor molecules used in this study

This deposition process has been introduced as a potential solution to naturally generate adequate

concentration gradients within the active layers of regular architecture OSC devices.²⁸ However, our EDS results clearly demonstrate that this is not always the case and that polymer crystallinity and molecular movement upon annealing have to be taken into account when correlating vertical concentration gradients and device performances. In fact, in this book chapter, we will first review our previous works which demonstrate that the vertical concentration gradient in SD-OSCs can be tuned through mechanical process or formulation. EDS is not limited to SD-OSCs characterizations and, consequently, studies on regular and inverted bulk heterojunction OSCs (BHJ-OSCs) with two different donor-acceptor systems are presented focusing on correlations between device performances and vertical concentration gradients to understand, in particular, the effects of post-annealing and the solvent used for the active layer deposition.

Methods to generate the adequate vertical concentration gradients in P3HT:PCBM OSCs

In SD-OSCs, the generation of the adequate concentration gradients relies on the fact that the polymer electron donor (e.g. P3HT) is practically insoluble in some solvents for fullerene derivatives (e.g. PCBM). In practice, when spin-coating a PCBM solution in DCM on a P3HT layer, a small amount of P3HT is dissolved during the process. However, as DCM swells the P3HT underlying film, PCBM can gradually diffuse into the P3HT network thus generating, theoretically, a vertical concentration gradient with P3HT-rich and PCBM-rich layers, respectively at the bottom and top of the active layer. In 2011, Lee *et al.* demonstrated that such a gradient can be observed in the as-cast pseudo-bilayer films but that, upon annealing and the induced molecular rearrangement, BHJ-like morphologies are obtained.¹⁶ In their study, they performed their analysis using neutron reflectometry with samples prepared by depositing the active layer on SiO₂ substrates. As the profiles obtained by reflectometry correspond to average data over large areas, it is hard to verify whether BHJ-like domains or multilayers (P3HT-rich and PCBM-rich layers) are formed. The EDS cross-section in Figure 7.1 clearly indicates that it is the latter. Nonetheless, the study by Lee *et al.* reveals that, although it is necessary to increase the crystallinity of donor and acceptor materials, the annealing process is detrimental in terms of quality of the vertical concentration gradient. Here, after presenting two different methods to form adequate vertical concentration gradients even after annealing in SD-OSC by adjusting the polymer crystallinity and its compatibility with PCBM, we will study the effect of annealing on the BHJ-OSC system in which the molecules are initially deposited at the same time.

Controlling the vertical concentration gradient with amorphous P3HT in SD-OSC active layers

As polymer crystallinity plays an essential role in the positive charge (hole) transport properties in OSCs, regioregular P3HT (RR-P3HT) is commonly used as electron donor with respect to its amorphous regiorandom equivalent (RRa-P3HT).²⁹ During the annealing process, a variety of parameters have to be taken into account to understand the changes in morphology which occur within the OSC active layer. The molecular spatial and morphological rearrangement is highly dependent on the interactions of the active molecules (P3HT and PCBM) with the interfacial materials and with each others. In fact, RR-P3HT and RRa-P3HT will likely interact in different manners with PCBM as their intrinsic properties (e.g. surface free energy or solubility in DCM) can be notably different.^{30,31} The common opinion on P3HT:PCBM films is that upon annealing and the

consequent increase in crystallinity of both polymer and fullerene derivative, we observe an increment of the degree of phase separation between the two materials. In other words, a more amorphous polymer phase is more likely to lead to intimate mixing with PCBM thus decreasing the amount of phase separation even after annealing.

RRa-P3HT is an amorphous material which does not crystallize even when annealed at high temperatures. However, due to this amorphous nature and the consequent lower hole transport properties and higher solubility in DCM, RRa-P3HT based SD-OSCs do not exhibit high performances. From a thermodynamic point of view, RRa-P3HT should be more compatible with PCBM as compared to RR-P3HT as the surface free energies for regioregular polythiophenes (e.g. RR-P3HT), regiorandom polythiophenes (e.g. RRa-P3HT) and PCBM are of approximately 21, 29 and 38 mN/m, respectively.^{30,31}

In order to use RRa-P3HT to obtain the adequate vertical concentration gradient while maintaining high hole mobilities in SD-OSC active layers, we therefore used the following strategy: we first deposited RR-P3HT:RRa-P3HT blends varying the wt% of RRa-P3HT with respect to the total P3HT weight and then, in a second step, deposited the PCBM solution from DCM on top of the blended P3HT thin films. The resulting device performances after a post-electrode deposition annealing step exhibit large improvements with *PCE* increasing from 3.1% (RR-P3HT only) up to 3.8% (15 RRa-P3HT wt%). The fabrication process and device *PCEs* are summarized in Figure 7.2.²¹

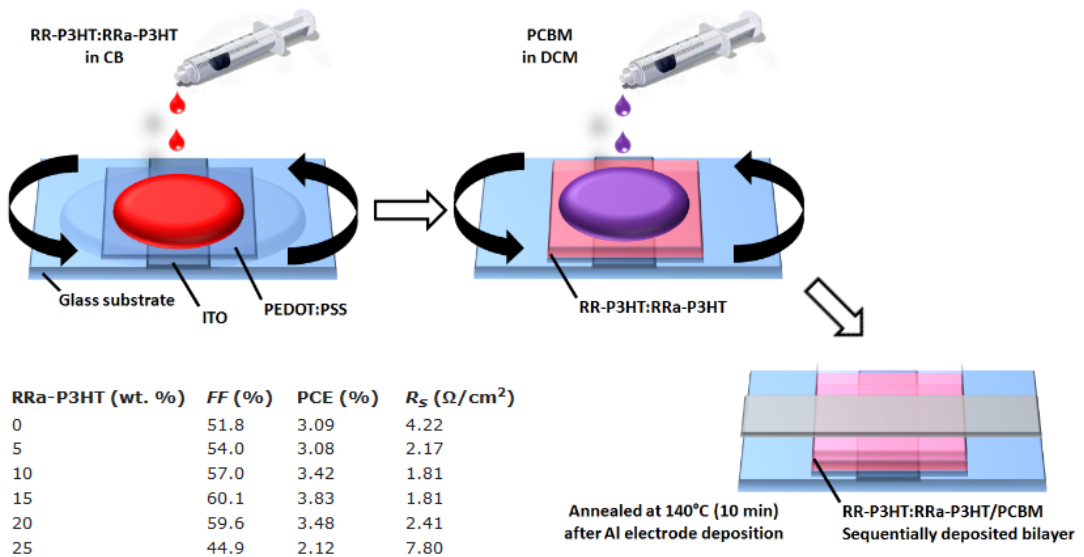


FIGURE 7.2

Schematic representation of the RR-P3HT+RRa-P3HT:PCBM SD-OSCs and their device performances

Similarly to the *PCEs*, the *FF* exhibits a large increase with values reaching approximately 60% for 15 and 20 RRa-P3HT wt% devices. Together with the decrease in series resistance (R_s) of the devices, this suggests that adequate donor-acceptor concentration profiles are obtained for 15-20 RRa-P3HT wt% devices. Here, we used EDS cross-section characterization to analyze the correlation between the addition of RRa-P3HT to the electron donor layer, the vertical concentration profiles and the device performances (Figure 7.3). We can clearly observe that the P3HT layer formed at the top of the active layer in RR-P3HT:PCBM SD-OSCs gradually disappears upon addition of RRa-P3HT.

Up to 5 RRa-P3HT wt%, the PCBM-rich layer is still trapped between two P3HT-rich layers but in 10 to 25 RRa-P3HT wt% SD-OSCs, we can recognize the formation of a PCBM buffer layer which gradually increases with RRa-P3HT content. Note that, while a thin PCBM layer can extremely enhance the performances of OSCs, a thick buffer layer, on the other hand, will have a negative effect as the distance between the donor-acceptor interface (where electrons are photogenerated) and the cathode becomes larger. A schematic representation of the active layer profiles obtained for the various RRa-P3HT concentrations is displayed in Figure 7.3, which confirms that the ideal vertical concentration gradient in regular P3HT:PCBM SD-OSCs should be as follows: P3HT buffer layer (approx. 15-20 nm) / mixed P3HT:PCBM layer with increasing PCBM content (approx. 60-80 nm) / PCBM buffer layer (approx. 15-20 nm). This ideal profile is obtained for 20 wt% of additional RRa-P3HT which, however, displays lower *PCEs* compared to 15 wt% devices. This is explained by the fact that the molar extinction coefficient of RRa-P3HT is lower than that of RR-P3HT and consequently, the amount of photogenerated charges decreases (lower *Jsc*).

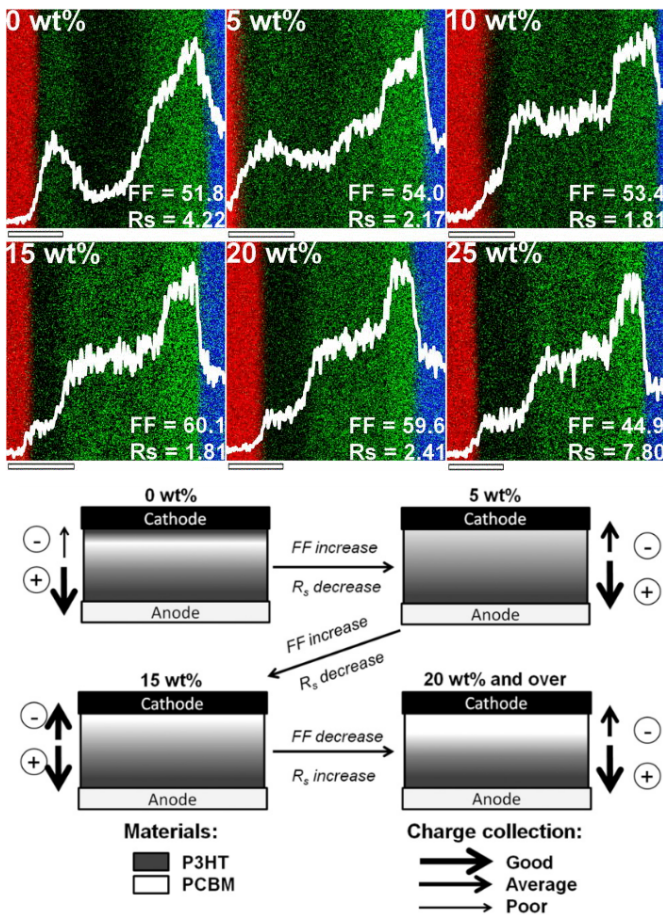


FIGURE 7.3

EDS elemental mapping of the RR-P3HT+RRa-P3HT:PCBM SD-OSCs and schematic representation of the evolution of *FF* and R_s with respect to the vertical concentration gradient in the devices. In the EDS images, red, green, blue and black colors indicate the aluminum (Al), sulfur (S), indium (In) and carbon (C), respectively. The white line indicates the intensity of the S element. Figure 7.3 was adapted from references [21] and [23] with permissions. Copyright 2012, AIP Publishing LLC. Copyright 2014, Elsevier B.V.

Hence, achieving the ideal vertical concentration gradient while solely using RR-P3HT should lead to higher device performances. This can be achieved by adapting the P3HT layer deposition process in order to modify its crystallinity. For example, spin-coating the P3HT layer from higher boiling point solvents has proven to be an efficient method to control the formation of vertical concentration gradients without using RRa-P3HT.²⁴ Post-deposition processes can also be applied to modify the crystallinity of the P3HT layer by using techniques such as rubbing (results presented in the following section). As RRa-P3HT will not be used in the rest of this book chapter, from this point, P3HT refers to RR-P3HT.

Ideal vertical concentrations in increased polymer crystallinity SD-OSC devices

Rubbing polymer layers is a method widely used in the liquid crystal display industry as it allows for orientation of the polymer chains which, in turn, induces epitaxial growth of liquid crystals formed on these oriented templates.³² As polymer chain orientation favors crystalline growth, the impact on the polymer layer crystallinity is also consequent and provides means to control the penetration of PCBM within the P3HT network. In fact, as mentioned previously, in P3HT:PCBM SD-OSC active layers, the adequate vertical concentration gradient is obtained prior to the annealing step but molecular rearrangement (mainly due to P3HT crystallization) induces the formation of a P3HT-rich layer close to the top cathode, which is detrimental for device performances as it prevents efficient electron collection. However, if P3HT already has a high degree of crystallinity prior to annealing, the movement of P3HT and PCBM molecules becomes more limited and therefore, the pre-annealing morphologies may be maintained even after the annealing process. On the other hand, we have to keep in mind that with increasing crystallinity, P3HT becomes more resistant to DCM and therefore, less diffusion of PCBM within the P3HT network could be expected. The P3HT films were rubbed 0 (reference), 3, 5 and 10 times prior to PCBM layer deposition to observe the impact of rubbing on the device performances (Figure 7.4).²²

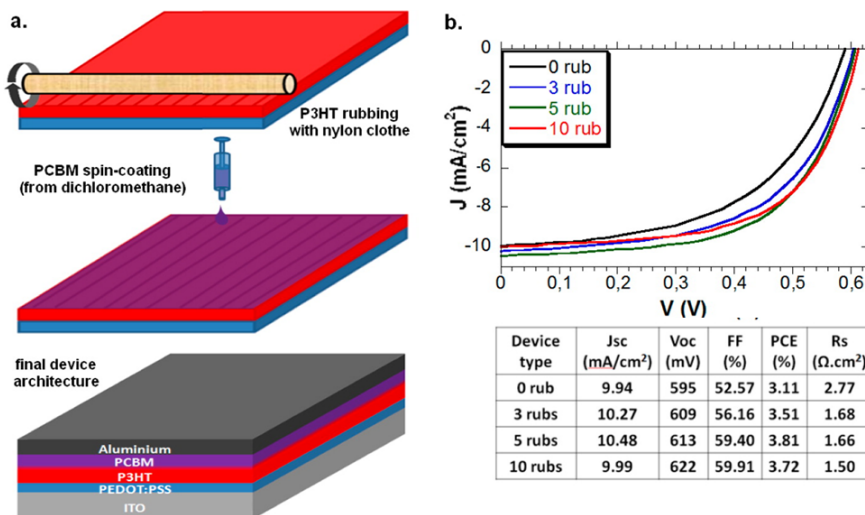


FIGURE 7.4

Schematic representation of the rubbed P3HT:PCBM SD-OSCs fabrication process and the resulting device performances. Figure 7.4 was adapted from reference [22] with permission. Copyright 2012, American Chemical Society.

The photovoltaic parameters clearly exhibit a gradual increase in open-circuit voltage (V_{oc}), FF and PCE with increasing rubbing times. J_{sc} , on the other hand, increases up to 5 rubs but then decreases at 10 rubs while the R_s constantly decreases with increasing rubbing numbers. Assuming that crystallinity of P3HT increases with rubbing times, we should be able to observe an increasingly adequate concentration gradient within the active layers of rubbed devices. Figure 7.5 displays the three EDS profiles obtained for 0, 5 and 10 rubs, respectively.

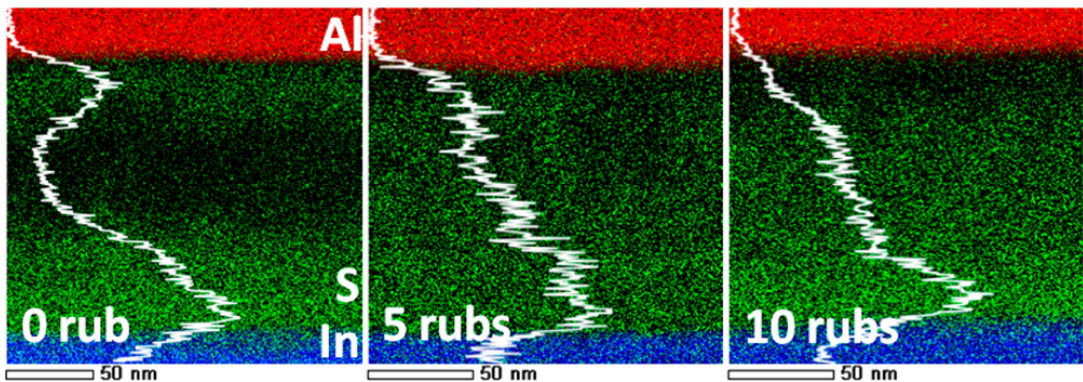


FIGURE 7.5

EDS elemental mapping of P3HT:PCBM SD-OSCs with the P3HT layer rubbed 0, 5 and 10 times prior to PCBM deposition and post-electrode deposition annealing. In the EDS images, red, green, blue and black colors indicate the aluminum (Al), sulfur (S), indium (In) and carbon (C), respectively. The white line indicates the intensity of the S element. Figure 7.5 was reproduced from reference [22] with permission. Copyright 2012, American Chemical Society.

By using the EDS profiles, the correlation between the vertical concentration gradient and the device performances can, once again, be easily understood. Similarly to the results obtained in the previous section, the P3HT-rich layer at the top of the active layer gradually disappears upon increasing rubbing times. In fact, unlike the addition of RRa-P3HT, here, the optical properties and energetic levels of the donor material remain the same and therefore, it becomes relevant to compare J_{sc} and V_{oc} in addition to FF , R_s and $PCEs$. For instance, as the top P3HT-rich layer disappears, the amount of reverse saturation current density (J_0) will also decrease. Taking into account the fact that J_{sc} in the devices does not change notably (up to around 5%), and that V_{oc} has a linear relationship to $\ln(J_{sc}/J_0)$, the increase in V_{oc} is consistent with a decrease of leak current in the devices.³³ On the other hand, the EDS images and sulfur profiles demonstrate that up to 5 rubs, P3HT and PCBM still display a relatively intimate mixing (small domain formation due to PCBM diffusion within the P3HT network) with a continuous P3HT:PCBM vertical gradient while the 10 times rubbed samples display an abrupt decrease in P3HT concentration due to the lower mixing of P3HT and PCBM in these samples. Consequently, a lower J_{sc} is obtained for the 10 times rubbed films as compared to the 3 and 5 times rubbed ones. As the adequate vertical concentration gradient is formed, a large increase in FF can also be observed with maximum values around 60% obtained when a thin PCBM buffer layer is formed. Note that due to the lower J_{sc} in 10 times rubbed devices, the highest PCE for rubbed SD-OSCs is obtained for 5 rubs with average and maximum $PCEs$ reaching 3.81 and 3.99%, respectively.

Our results once again demonstrate that EDS can be a powerful tool to understand the morphological evolution of P3HT:PCBM SD-OSC active layers and, in particular, select the

conditions to obtain the adequate crystallinity of the polymer and fabricate highly efficient OSC devices. In fact, a similar approach was recently introduced by Seok *et al.* using solvent additives to obtain the adequate morphology in SD-OSCs based on a higher performing polymer:fullerene combination.²⁶ EDS cross-section profiles, which, up to 2015, were rarely used when characterizing the active layer morphologies of SD-OSCs, now seem to have become a reliable analytical method to understand the device characteristics and allowed to fabricate SD-OSCs with *PCE* up to 7.12% using the high performance polymer:fullerene combination. However, this analytical technique is not limited to the use of SD-OSCs and can also be applied to BHJ-OSCs to provide additional information on the active layer morphology as we will see in the following sections.

Investigating the effect of thermal annealing on P3HT:PCBM BHJ-OSC performances

Unlike SD-OSCs, in BHJ-OSCs, the donor and acceptor materials are blended prior to deposition. During the deposition process, P3HT and PCBM phase separate not only horizontally but also vertically to generate P3HT- and PCBM-rich domains. The formation of large crystalline domains has opposing effects on the *J_{sc}* and *FF* of BHJ-OSCs. In fact, large crystalline domains result in a decrease in donor-acceptor interface and consequently, a decrease in the quantity of photogenerated charges. On the other hand, highly crystalline domains will lead to much more efficient charge transport which will increase the *FF* of the devices. The formation of large clusters of PCBM can be easily detected using optical microscopy and constant efforts are made to optimize the annealing conditions for an adequate balance between increased crystallinity and large domain formation leading to enhanced device performances.³⁴ In particular, thermal annealing is a valuable method to control the crystalline growth through annealing times or temperatures and understand the molecular rearrangement which occurs during this post-deposition process.^{34,35} Previous studies on P3HT:PCBM BHJ-OSCs confirmed that, similarly to SD-OSCs, a particular attention should also be given to vertical concentration gradients and that thermal annealing as well as interfacial interactions (e.g. substrate/active layer interface) play a major role to improve device performances.^{36,37} In fact, several methods to readily achieve vertical concentration gradients either in situ or through controlled deposition and post-deposition processes were recently introduced.^{15,37-39} In these studies, the vertical concentration gradient is studied using surface analysis (top and bottom surfaces) or comparing the surface and bulk properties (GI-XRD). As it fully probes the devices in a non-destructive layer-by-layer approach, spectroscopic ellipsometry is now widely used as one of the preferential methods to analyze the vertical concentration gradients in BHJ-OPV devices.²⁰ However, spectroscopic ellipsometry largely depends on the used models and the quality of the fittings which have to be adapted to each material to obtain reliable data and therefore, cannot be considered as an easily implemented direct visualization systematical analytical tool. Here, we will demonstrate how EDS can provide precise information on the vertical concentration gradient formation and its evolution upon thermal annealing in BHJ-OSCs allowing us to understand whether the performance improvement is related to vertical donor-acceptor distribution.

The effects of thermal annealing and interface interactions on the P3HT:PCBM active layer morphologies are highly dependent on each other. In fact, attraction/repulsion interactions at the interfaces represent one of the major driving forces for PCBM redistribution within the active layer thickness. To verify the effect of annealing on the P3HT:PCBM active layers in regular architectures, we deposited a 120 nm thick P3HT:PCBM layer from CB and compared the EDS profiles for 3 samples on Glass/ITO/PEDOT:PSS substrates (Figure 7.6):

- unannealed: spin-coated active layer without any thermal treatment

- pre-annealed: active layer annealed prior to Al deposition (active layer/air interface)
- post-annealed: active layer annealed after Al deposition (active layer/Al interface)

Figure 7.6 summarizes the sulfur profiles observed for the active layer before and after annealing along with a schematic representation of the sample fabrication.

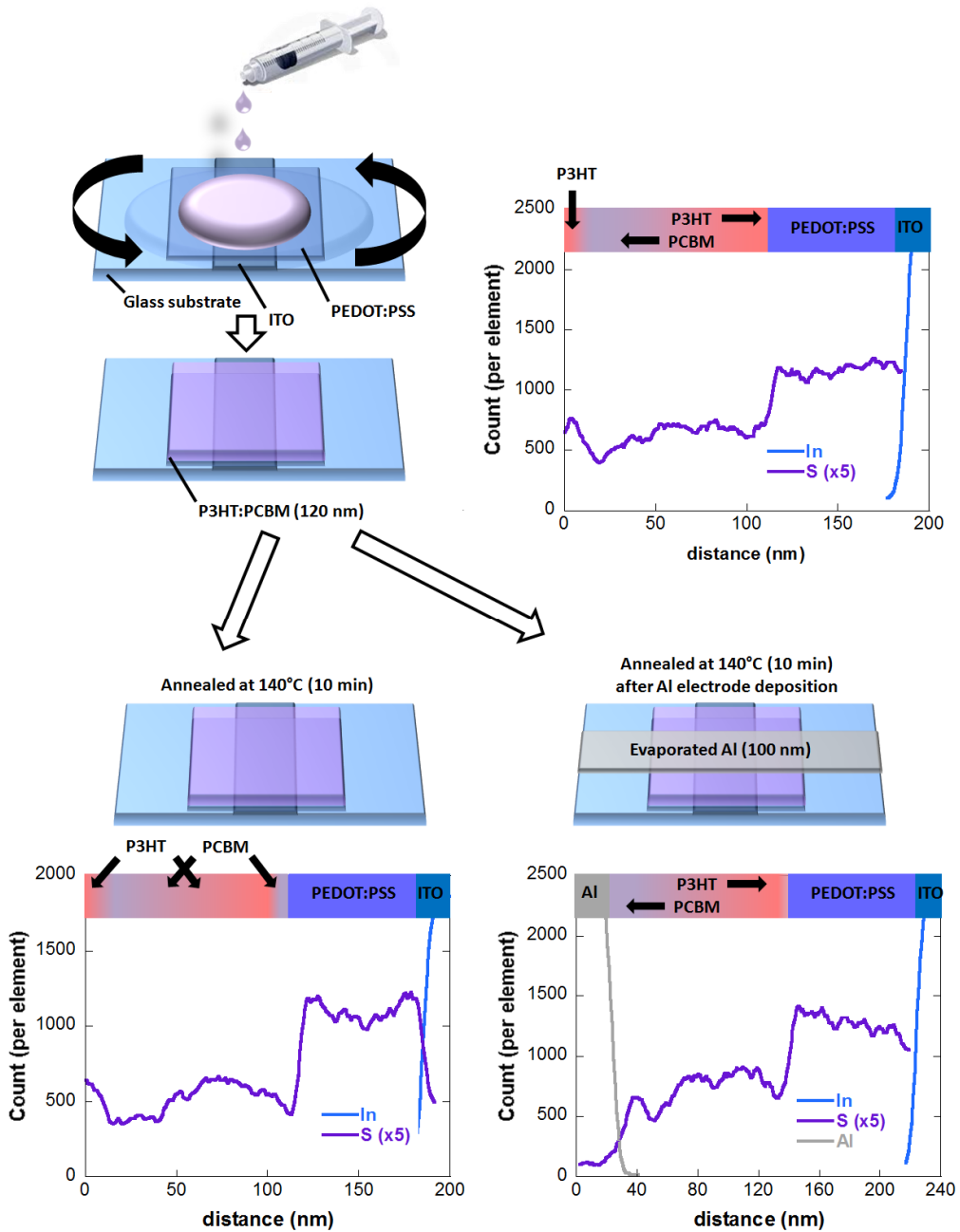


FIGURE 7.6 Schematic representation of the process to fabricate P3HT:PCBM BHJ-OSCs and resulting EDS profiles corresponding to the various fabrication steps

In the unannealed active layer, we can clearly observe that, while the bottom part of the film displays a rather homogeneous (flat) donor:acceptor concentration, a 10-15 nm thick PCBM-rich layer is trapped by a P3HT-rich layer at the active layer/air interface. The electrons generated in the PCBM-rich layer are consequently trapped below a hole-only layer which should result in a relatively low electron extraction efficiency. During the film deposition, PCBM diffuses away from the interface with air suggesting a higher affinity of P3HT with air. Consequently, upon annealing in the same conditions (top surface in contact with air), the thin layer at the top interface becomes more concentrated in P3HT and a PCBM-rich layer appears at the bottom of the film (active layer/PEDOT:PSS interface) suggesting that PCBM has slightly more affinity with PEDOT:PSS as compared to air.

On the other hand, once the aluminum cathode is deposited on the surface of the active layer, the post-annealing induces a different rearrangement of the molecules along the vertical direction of the active layer. A PCBM-rich layer is formed at the top interface with the cathode and a much smaller drop of P3HT concentration at the PEDOT:PSS interface can be observed. In fact, the profile obtained for the post-annealed samples demonstrate an almost adequate concentration gradient for efficient charge extraction and therefore, higher FF from the post-annealed devices should be expected. Figure 7.7 confirms that upon post-annealing (after Al deposition), a large increase in FF can be observed in the devices.

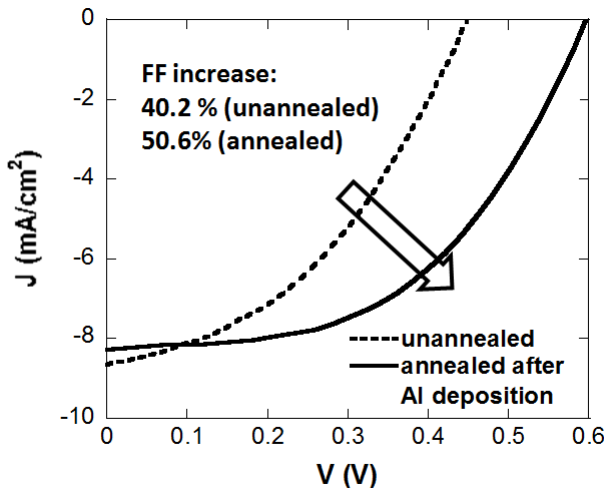


FIGURE 7.7

J - V curves of unannealed and annealed P3HT:PCBM BHJ-OSCs with a regular device architecture

In fact, the formation of an adequate vertical concentration gradient not only increases the FF but also the V_{oc} in these devices. The V_{oc} in the devices highly depend on the energetic levels of the donor and acceptor molecules which may vary due to aggregate formation during thermal annealing. However, the formation of a PCBM-rich layer at the interface with the cathode also induces a large decrease in J_0 , which, in turn, increases the V_{oc} in the devices.^{33,40} In fact, our results are in perfect agreement with those previously published, in which similar device performances were explained by observing changes at the active layer/cathode interface using XPS measurements without, however, verifying that no other major changes could be observed within the bulk of the active layer.⁴⁰

Although vertical concentration gradients do play essential roles in improving device performances, enhanced FF and $PCEs$ can sometimes be unrelated to donor-acceptor distributions. For instance, in inverted BHJ-OSCs, no major change in vertical concentration gradient can be observed upon annealing (Figure 7.8) but FF up to 62% are achieved in annealed devices with inadequate vertical concentration gradients.

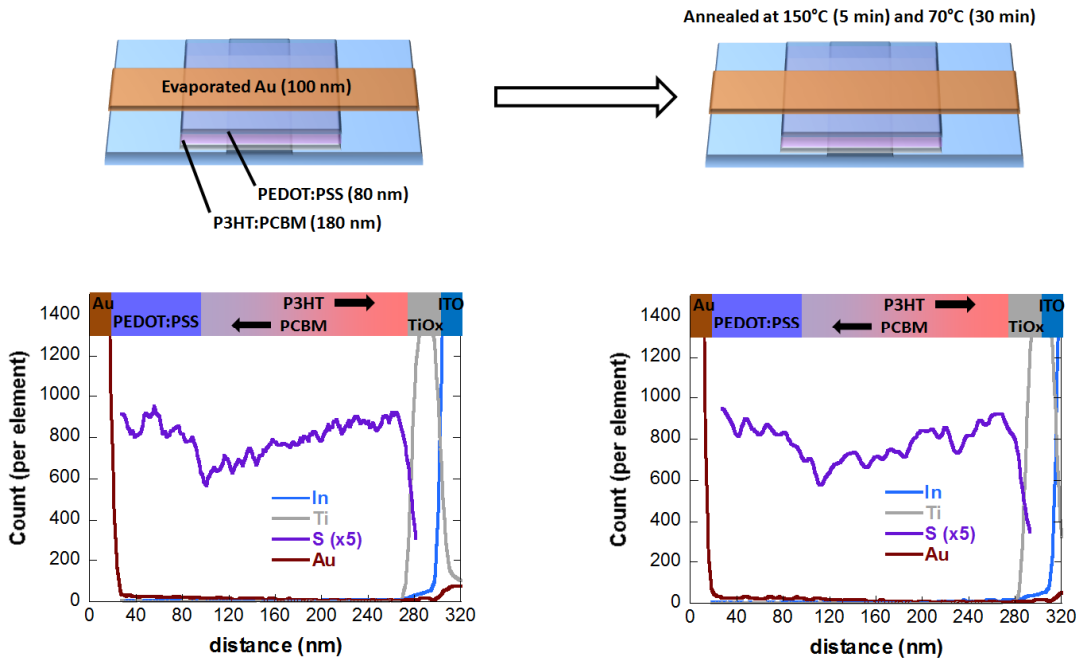


FIGURE 7.8

Schematic representation and EDS profiles of P3HT:PCBM inverted architecture BHJ-OSCs before and after a two-step annealing

The increased performances upon annealing in inverted BHJ-OSCs are simply due to the fact that PEDOT:PSS is also annealed during the active layer annealing, thus providing a much more efficient hole collection layer. Although they do not provide a clear evidence for the device performance improvement, the EDS profiles on unannealed and annealed active layers indicate that P3HT has a strong affinity with TiOx. The higher device performances observed for inverted devices (FF and PCE above 62 and 3.2%, respectively) compared to regular architectures with the adequate vertical concentration gradient (FF and PCE of 50.6 and 2.4%, respectively) strongly suggest that even higher performances could be obtained in inverted devices which display the adequate concentration gradient profiles. While thermal annealing does not seem to have a positive effect, in the next section, we will explore whether changing the interface materials (hole and electron transporting layers) or the solvents for active layer deposition can lead to adequate vertical donor-acceptor profile in PNTz4T: Phenyl- C_{71} -butyric acid methyl ester ($PC_{71}BM$) active layers.

Correlation between fabrication conditions, concentration gradient and device performances in high efficiency PNTz4T:PC₇₁BM BHJ-OSC devices

In the previous section of this chapter, we verified that EDS elemental mapping of P3HT:PCBM cross-sections is a powerful tool to understand the increase or decrease in P3HT based OSC. This analytical technique is not limited to the study of P3HT based systems but can be applied to virtually any electron-donor:electron-acceptor system as long as one of the active molecules contains at least one distinguishable atom. Recent progress in OSC has demonstrated the potential of wide bandgap copolymers as electron-donors in both regular and inverted device architectures.¹² For instance, the PNTz4T:PC₇₁BM combination gave *PCEs* as high as 8.5 and 10.1% for regular and inverted device architectures, respectively.^{3,13} In fact, these device performances are not only related to high *Jsc* (wide and strong absorption from the polymer combined with a fullerene derivative absorbing in the visible) but also to extremely high *FFs* obtained in the devices. Surprisingly, the highest *FF* is, once again, obtained for inverted device architectures in which the active layer is deposited on zinc oxide (ZnO) coated ITO substrates even though the vertical concentration gradient of these active layers is rather flat for inverted device architectures (PNTz4T distributed almost homogeneously along the vertical direction). As PNTz4T is a polymer with an extremely high crystallinity, thermal annealing of the active layer, even at relatively low temperatures, results in large phase separation between electron-donor and electron-acceptor domains. However, using solvents with different boiling temperature should give us the opportunity to compare various degrees of crystallinities in the polymer:fullerene blends.

Multilayer structures in PNTz4T:PC₇₁BM films deposited on TiOx coated ITO substrates

Here, we study the deposition of PNTz4T:PC₇₁BM active layers on TiOx using two solvents with different boiling temperatures, namely, CB and 1,2-Dichlorobenzene (DCB). Their boiling temperatures are 131 and 180.5 °C, respectively. Although thermal annealing cannot be performed on PNTz4T:PC₇₁BM active layers, using a higher boiling point solvent induces a slower drying of the film which should allow for the polymer chains (and fullerene derivative molecules) to arrange with a higher degree of order provided that the polymer is similarly soluble in both solvents. As presented in Figure 7.9, a peculiar donor-acceptor vertical concentration gradient is formed when depositing the films from CB. The EDS sulfur profiles clearly demonstrate that a PNTz4T-rich layer is trapped between two PC₇₁BM-rich layers present at both the active layer top and bottom interfaces. This represents the ideal situation for efficient electron percolation towards the bottom cathode. However, the hole percolation to the top anode becomes highly unlikely and therefore, relatively low *FF* are expected. Furthermore, due to the large phase separation into a PC₇₁BM-PNTz4T-PC₇₁BM trilayer morphology, the amount of photogenerated charges is limited (decrease in donor-acceptor interface) which should result in a decrease in *Jsc*. In fact, comparing the device performances of these active layers deposited on TiOx “Figure 7.9” with our previous studies with ZnO covered ITO cathodes³, we can clearly observe a decrease in *Jsc* from 16.2 to 13.98 mA/cm² for 200 nm thick active layers prepared on ZnO and TiOx, respectively. The effect on the *FF* is even stronger with a drop in *FF* value from 73.1 to 49.0% for ZnO and TiOx devices, respectively. The drop in *FF* is also due to the fact that we use PEDOT:PSS hole collection layers instead of MoO₃ layers to obtain data that are confrontable with the data from the regular device architectures (see following section). Note that the EDS profiles for PNTz4T:PC₇₁BM active layers prepared on ZnO

exhibit a rather flat donor:acceptor vertical distribution with only a very slight gradient (slightly more polymer towards the bottom of the film).

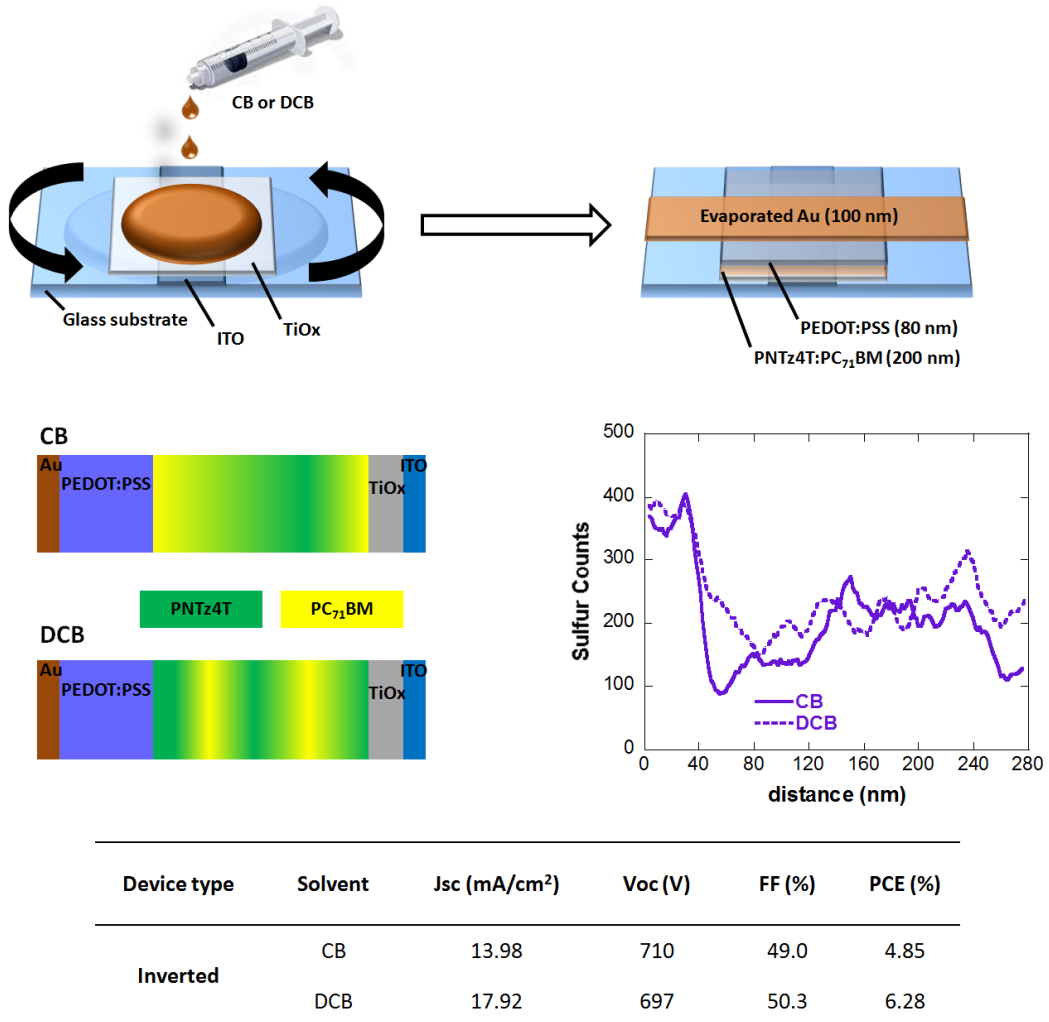


FIGURE 7.9

Schematic representation of the process to fabricate PNTz4T:PC₇₁BM inverted BHJ-OSCs and resulting EDS profiles

On the other hand, the EDS profile of the active layer deposited on TiOx from DCB displays a multilayer structure with numerous thin alternating PNTz4T-rich and PC₇₁BM-rich layers. Unlike the PNTz4T:PC₇₁BM thin film deposited from CB in which a large vertical phase separation can be observed, the active layer deposited from DCB displays much smaller domains with no particular preference for the fullerene to move at either interfaces. This contradicts the assumption that longer drying times (in films deposited from DCB) will lead to larger phase separation. Our hypothesis is that the polymer is simply more soluble in DCB as compared to CB, thus leading to better initial mixing conditions and consequently, smaller but more crystalline aggregate formation. In fact, the *J*_{sc} measured for TiOx DCB devices reaches an average value of 17.9 mA/cm², which is

even higher than the one obtained for flat vertical concentration gradient films obtained on ZnO (with a J_{sc} of 16.2 mA/cm²) confirming that a higher level of intimate mixing between PNTz4T and PC₇₁BM is achieved. Therefore, another common assumption, namely, that alternating layered structures are detrimental to device performances, may have to be reconsidered after closely analyzing our samples. However, the FF of these devices remains very low in comparison to the films deposited on ZnO as a result of a higher probability of charge recombination due to the slightly unfavorable concentration gradient and the multilayered structure as well as the less efficient unannealed PEDOT:PSS hole collection layer (compared to evaporated MoO₃). Overall, the slightly higher polymer concentration towards the bottom of the film suggests that, similarly to P3HT, regular devices may provide higher FF as compared to inverted architectures. This assumption, however, does not take into account the polymer crystallite orientation which, as demonstrated in our previous study, plays an essential role in terms of hole transport to the anode and explains the higher FF obtained in inverted architectures using ZnO covered ITO substrates.

Comparison between continuous vertical concentration gradients and multilayered structures in PNTz4T:PC₇₁BM regular architecture devices

Figure 7.10 exhibits typical EDS profiles obtained for active layers deposited on PEDOT:PSS layers from either CB or DCB. Similarly to inverted structures using ITO/TiO_x cathodes, rather than the boiling temperature of the solvent, the effect of the polymer solubility can be clearly observed. For the thin films deposited from DCB (in which both the polymer and the fullerene derivative are highly soluble), the sulfur profile confirms that a continuous decrease in PNTz4T concentration can be observed along the vertical direction in the cross-section of the device. The active layer deposited from CB also contains a higher concentration of PNTz4T close to the PEDOT:PSS underlying layer with, however, the formation of some alternating PNTz4T-rich and PC₇₁BM-rich layers. As these donor- and acceptor-rich domains still contain a fairly large amount of the other material, percolation can still occur but in a less efficient way as compared to the continuous profiles obtained for active layers spin-coated from DCB. In both cases, the top and bottom parts of the active layers (interfaces with the LiF/Al anode and ITO/PEDOT:PSS, respectively) contain a higher concentration of PC₇₁BM and PNTz4T, respectively, which should lead to efficient charge extraction properties at the interfaces. This is well reflected in the FF of the devices with a slightly higher average value obtained for DCB devices in comparison with their CB counterparts. Additionally, these two layers formed at the interfaces remarkably reduce the leak currents (J_0) which is well correlated with the increase in V_{oc} observed for regular device architectures as compared to the inverted devices presented in the previous section.

Interestingly, for both regular and inverted structures prepared in this study, the devices prepared from CB exhibit a V_{oc} value which is approximately 13 mV higher to those prepared using DCB based solutions. This slight change in V_{oc} may be due to slightly different molecular organization of the polymer chains obtained in both cases. In fact, as observed by Osaka et al., in PNTz4T solutions prepared in CB, as the polymer is barely soluble at room temperature, the absorption spectra of the solution at room and high temperatures display a large shift.¹² This is typically ascribed to a change in interchain interactions with the red shifted spectrum (room temperature) corresponding to polymer aggregates in solution while chains dispersed in the solution (high temperature) are reflected by the blue shifted spectrum. These measurements suggest that the polymer chains are already in an aggregated state before the spin-coating process starts in the case of CB. The EDS profile support the assumption that the polymer is more soluble in DCB as a layered structure is formed in CB while DCB active layers display a much smoother profile. In crystalline structures, as

charges can delocalized on a wider scale, the HOMO and LUMO of the organic semi-conductors will be stabilized which may slightly increase the HOMO_{DONOR}-LUMO_{ACCEPTOR} gap, a value closely related to the V_{oc} . The more crystalline PNTz4T obtained in regular device architectures when the active layers are spin-coated from CB therefore leads to a V_{oc} of 751 mV which, together with the high J_{sc} generated from the large donor-acceptor interface in the CB devices (alternating donor-/acceptor-rich layers) results in average $PCEs$ of 8.5%. Although the adequate profile obtained in devices coated from DCB produce a higher FF , the lower V_{oc} and J_{sc} (compared to CB devices) lead to a slightly lower average PCE of 8.3%. Concentration profiles can therefore help us to understand and explain various aspects of the device performances. However, all the device parameters cannot always be explained only by using EDS cross-section profiles. In fact, using PNTz4T:PC₇₁BM active layers in inverted device architectures (ITO/ZnO/ PNTz4T:PC₇₁BM/MoO₃/Ag), FFs and $PCEs$ over 70 and 10%, respectively, have been obtained. The increase in performances compared to our regular devices was not related to the formation of an ideal donor-acceptor concentration gradient but to the formation of a face-on/edge-on crystallite concentration gradient. Although EDS can precisely reflect the materials concentration in the various parts of the thin films, it cannot be used to obtain direct information on the crystallinity and crystallite orientation of the molecules involved. Therefore, to completely understand the various active layers studied by OSC scientists, a combination of analytical techniques are required. Our work confirms that EDS can be one of these analytical techniques which should be systematically applied to active layers and especially, recently introduced donor-acceptor systems for which reliable data on the vertical concentration gradients has not yet been presented.

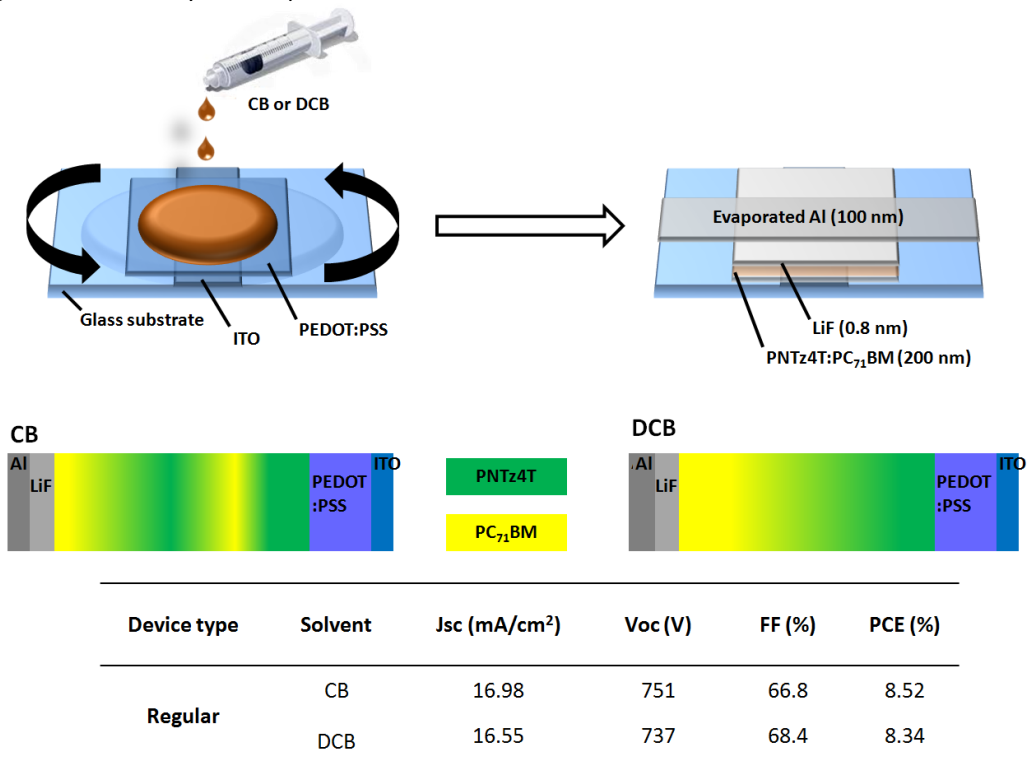


FIGURE 7.10

Schematic representation of the process to fabricate PNTz4T:PC₇₁BM regular BHJ-OSCs and their EDS schematic profiles

Conclusion

In summary, we have studied the active layer cross-sections of various OSC devices using EDS elemental mapping to understand the influence of the process on the formation of a vertical concentration gradient. Furthermore, the studies introduced here allowed us to correlate these vertical concentration profiles with the device performances, in particular, using P3HT:PCBM and PNTz4T:PC₇₁BM active layers which correspond to the state-of-the-art and recently introduced high efficiency materials' combination, respectively. A particular attention was given to the evolution of the *FF* using a variety of processes ranging from simple thermal annealing to mechanical processes such as rubbing.

In fact, our experiments on P3HT:PCBM SD-OSCs confirmed that, upon thermal annealing of active layers using the common deposition process, the adequate vertical concentration profile is not obtained. However, it can be obtained by either adding amorphous P3HT to the electron-donor layer (increasing the miscibility of the polymer with PCBM) or by rubbing it (blocking the diffusion of molecules during thermal annealing). The devices with the adequate vertical concentration gradients showed remarkable increases in both *FF* and *PCE* reaching values of approximately 60 and 4%, respectively.

In BHJ-OSCs, we further observed the effect of annealing before and after cathode deposition. The active layer deposited on a PEDOT:PSS layer is therefore annealed either with a top air or aluminum interface. With the latter, we could observe the formation of a PCBM-rich layer at the top of the active layer which reduces the reverse saturation current leading to increases in *V_{oc}* and *FF*.

To obtain high performing OSC devices, completely understanding the morphology of the active layer is absolutely necessary. From our previous study, we have demonstrated that the molecular orientation concentration is favorable to inverted device architectures. However, by the usual deposition processes (spin-coating), adequate vertical donor-acceptor gradients are hardly obtained in inverted architectures. Here, we understood that alternating donor-rich and acceptor-rich domains may not necessarily be detrimental to the *FF* in the devices. Much higher *FF* and *PCE* could be expected if both the adequate crystallite orientation gradient and donor-acceptor gradient are achieved in newly introduced polymer-based OSCs. To verify whether these conditions are met, we believe that EDS elemental mapping represents a valuable analytical tool to understand which processes could be used for the fabrication of OSCs with *PCEs* over 15%.

Acknowledgements

This work was supported by Grant-in-Aid for Scientific Research on Innovative Areas (grant no. 20108012, "pi-Space") from the Ministry of Education, Culture, Sports, Science, and Technology, Japan, by JSPS KAKENHI Grant Number 26889029 and by the JGC-S Scholarship Foundation (Research Grant for Young Researcher).

References

1. R. R. Søndergaard, M. Hösel and F. C. Krebs. Roll-to-Roll fabrication of large area functional organic materials. *J. Polym. Sci. B* **2013**, *51*, 16–34.
2. W. Cao and J. Xue. Recent progress in organic photovoltaics: device architecture and optical design. *Energy Environ. Sci.* **2014**, *7*, 2123-2144.

3. V. Vohra, K. Kawashima, T. Kakara, T. Koganezawa, I. Osaka, K. Takimiya and H. Murata. Efficient inverted polymer solar cells employing favourable molecular orientation. *Nature Photon.* **2015**, *9*, 403-408.
4. Y. Liu, J. Zhao, Z. Li, C. Mu, W. Ma, H. Hu, K. Jiang, H. Lin, H. Ade and H. Yan. Aggregation and morphology control enables multiple cases of high-efficiency polymer solar cells. *Nature Comm.* **2014**, *5*, 5293.
5. J.-D. Chen, C. Cui, Y.-Q. Li, L. Zhou, Q.-D. Ou, C. Li, Y. Li and J.-X. Tang. Single-Junction Polymer Solar Cells Exceeding 10% Power Conversion Efficiency. *Adv. Mater.* **2015**, *27*, 1035–1041.
6. J. Huang, J. H. Carpenter, C.-Z. Li, J.-S. Yu, H. Ade and A. K.-Y. Jen. Highly Efficient Organic Solar Cells with Improved Vertical Donor–Acceptor Compositional Gradient Via an Inverted Off-Center Spinning Method. *Adv. Mater.* **2016**, *28*, 967–974.
7. C. W. Tang. Two-layer organic photovoltaic cell. *Appl. Phys. Lett.* **1986**, *48*, 183.
8. J. Roncali, P. Leriche and P. Blanchard. Molecular Materials for Organic Photovoltaics: Small is Beautiful. *Adv. Mater.* **2014**, *26*, 3821-3838.
9. L. Lu, T. Zheng, Q. Wu, A.M. Schneider, D. Zhao and L. Yu. Recent Advances in Bulk-Heterojunction Polymer Solar Cells. *Chem. Rev.* **2015**, *115*, 12666-12731.
10. M. T. Dang, L. Hirsch and G. Wantz. P3HT:PCBM, best seller in polymer photovoltaic research. *Adv. Mater.* **2011**, *23*, 3597-3602.
11. G. Zhao, Y. He and Y. Li. 6.5% Efficiency of Polymer Solar Cells Based on poly(3-hexylthiophene) and Indene-C60 Bisadduct by Device Optimization. *Adv. Mater.* **2010**, *22*, 4355-4358.
12. I. Osaka, M. Shimawaki, H. Mori, I. Doi, E. Miyazaki, T. Koganezawa and K. Takimiya. Synthesis, Characterization, and Transistor and Solar Cell Applications of a Naphthobisthiadiazole-Based Semiconducting Polymer. *J. Am. Chem. Soc.* **2012**, *134*, 3498–3507.
13. V. Vohra, K. Higashimine, K. Ohdaira, S. Tsuzaki and H. Murata. Comparative Study of Fullerene Derivatives Blended with a High Efficiency Naphthobisthiadiazole-Based Polymer for Organic Photovoltaic Applications. in *Chemical Science of π -electron Systems*; Akasaka, T.; Osuka, A.; Fukuzumi, S.; Kandori, H.; Aso, Y., Eds. Springer: Japan, **2015**; 575-588.
14. C.-W. Liang, W.-F. Su and L. Wang. Enhancing the photocurrent in poly(3-hexylthiophene)/[6,6]-phenyl C₆₁butyric acid methyl ester bulk heterojunction solar cells by using poly(3-hexylthiophene) as a buffer layer. *Appl. Phys. Lett.* **2009**, *95*, 133303.
15. S. Cho, K.-D. Kim, J. Heo, J.Y. Lee, G. Cha, B.Y. Seo, Y.D. Kim, Y.S. Kim, S.-Y. Choi and D.C. Lim. Role of additional PCBM layer between ZnO and photoactive layers in inverted bulk-heterojunction solar cells. *Sci. Rep.* **2014**, *4*, 4306.
16. K.H. Lee, P.E. Schwenn, A.R.G. Smith, H. Cavaye, P.E. Shaw, M. James, K.B. Krueger, I.R. Gentle, P. Meredith and P.L. Burn. Morphology of all-solution-processed “bilayer” organic solar cells. *Adv. Mater.* **2011**, *23*, 766-770.
17. K. Tvingstedt, K. Vandewal, F. Zhang and O. Inganäs. On the Dissociation Efficiency of Charge Transfer Excitons and Frenkel Excitons in Organic Solar Cells: A Luminescence Quenching Study. *J. Phys. Chem. C* **2010**, *114*, 21824-21832.
18. S.H. Park, A. Roy, S. Beaupré, S. Cho, N. Coates, J.S. Moon, D. Moses, M. Leclerc, K. Lee and A.J. Heeger. Bulk heterojunction solar cells with internal quantum efficiency approaching 100%. *Nature Photon.* **2009**, *3*, 297-302.
19. A. Tada, Y. Geng, Q. Wei, K. Hashimoto and K. Tajima. Tailoring organic heterojunction interfaces in bilayer polymer photovoltaic devices. *Nature Mater.* **2011**, *10*, 450-455.

20. M. Campoy-Quiles, T. Ferenczi, T. Agostinelli, P. G. Etchegoin, Y. Kim, T. D. Anthopoulos, P. N. Stavrinou, D. D. C. Bradley and J. Nelson. Morphology evolution via self-organization and lateral and vertical diffusion in polymer:fullerene solar cell blends. *Nature Mater.* **2008**, *7*, 158 – 164.
21. V. Vohra, K. Higashimine, T. Murakami and H. Murata. Addition of regiorandom poly(3-hexylthiophene) to solution processed poly(3-hexylthiophene):[6,6]-phenyl-C61-butyric acid methyl ester graded bilayers to tune the vertical concentration gradient. *Appl. Phys. Lett.* **2012**, *101*, 173301.
22. V. Vohra, G. Arrighetti, L. Barba, K. Higashimine, W. Porzio and H. Murata. Enhanced Vertical Concentration Gradient in Rubbed P3HT:PCBM Graded Bilayer Solar Cells. *J. Phys. Chem. Lett.* **2012**, *3*, 1820–1823.
23. V. Vohra, K. Higashimine, S. Tsuzaki, K. Ohdaira and H. Murata. Formation of vertical concentration gradients in poly(3-hexylthiophene-2,5-diyl): Phenyl-C61-butyric acid methyl ester-graded bilayer solar cells. *Thin Solid Films* **2014**, *554*, 41-45.
24. V. Vohra, B. Döring, K. Higashimine and H. Murata. Investigating the effect of solvent boiling temperature on the active layer morphology of diffusive bilayer solar cells. *Appl. Phys. Expr.* **2015**, *9*, 012301.
25. R. Fitzgerald, K. Keil and K. F. J. Heinrich. Solid-State Energy-Dispersion Spectrometer for Electron-Microprobe X-ray Analysis. *Science* **1968**, *159*, 528-530.
26. J. Seok, T. J. Shin, S. Park, C. Cho, J.-Y. Lee, D. Y. Ryu, M. H. Kim and K. Kim. Efficient Organic Photovoltaics Utilizing Nanoscale Heterojunctions in Sequentially Deposited Polymer/fullerene Bilayer. *Sci. Rep.* **2015**, *5*, 8373.
27. V. W. Bergmann, S. A. L. Weber, F. J. Ramos, M. K. Nazeeruddin, M. Grätzel, D. Li, A. L. Domanski, I. Lieberwirth, S. Ahmad, R. Berger. Real-space observation of unbalanced charge distribution inside a perovskite-sensitized solar cell. *Nat. Comm.* **2014**, *5*, 5001.
28. A. L. Ayzner, C. J. Tassone, S. H. Tolbert and B. J. Schwartz. Reappraising the need for bulk heterojunction in polymer-fullerene photovoltaics: the role of carrier transport in all-solution-processed P3HT/PCBM bilayer solar cells. *J. Phys. Chem. C* **2009**, *113*, 20050-20060.
29. R. Mauer, M. Kastler and F. Laquai. The Impact of Polymer Regioregularity on Charge Transport and Efficiency of P3HT:PCBM Photovoltaic Devices. *Adv. Funct. Mater.* **2010**, *20*, 2085–2092.
30. J. Jaczewska, I. Raptis, A. Budkowski, D. Goustouridis, J. Raczowska, M. Sanopoulou, E. Pamula, A. Bernasik and J. Rysz. Swelling of poly(3-alkylthiophene) films exposed to solvent vapors and humidity: Evaluation of solubility parameters. *Synth. Met.* **2007**, *157*, 726-732.
31. J.J. Michels and E. Moons. Simulation of Surface-Directed Phase Separation in a Solution-Processed Polymer/PCBM Blend. *Macromolecules* **2013**, *46*, 8693-8701.
32. S.I. Jo, Y. Kim, J.-H. Baek, C.-J. Yu and J.H. Kim. Highly polarized emission of the liquid crystalline conjugated polymer by controlling the surface anchoring energy. *Jpn. J. Appl. Phys.* **2014**, *53*, 03CD04.
33. A. Orimo, K. Masuda, S. Honda, H. Benten, S. Ito, H. Ohkita and H. Tsuji. Surface segregation at the aluminum interface of poly(3-hexylthiophene)/fullerene solar cells. *Appl. Phys. Lett.* **2010**, *96*, 043305.
34. D.E. Motaung, G.F. Malgas, S.S. Nkosi, G.H. Mhlongo, B.W. Mwakikunga, T. Malwela, C.J. Arendse, T.F.G. Muller and F.R. Cummings. Comparative study: the effect of annealing conditions on the properties of P3HT:PCBM blends. *J. Mater. Sci.* **2013**, *48*, 1763-1778.

35. G.A. Berriman, J.L. Holdsworth, X. Zhou, W.J. Belcher and P.C. Dastoor. Molecular versus crystallite PCBM diffusion in P3HT:PCBM blends. *AIP Advances* **2015**, *5*, 097220.
36. P.G. Karagiannidis, D. Georgiou, C. Pitsalidis, A. Laskarakis and S. Logothetidis. Evolution of vertical phase separation in P3HT:PCBM thin films induced by thermal annealing. *Mater. Chem. Phys.* **2011**, *129*, 1207-1213.
37. V. Vohra, T. Anzai, S. Inaba, W. Porzio and L. Barba. Transfer-printing of active layers to achieve high quality interfaces in sequentially deposited multilayer inverted polymer solar cells fabricated in air. *Sci. Tech. Adv. Mater.* **2016**, *17*, 530-540.
38. D.K. Susarova, P.A. Troshin, Y.L. Moskvin, S.D. Babenko and V.F. Razumov. Vertical concentration gradients in bulk heterojunction solar cells induced by differential material solubility. *Thin Solid Films* **2011**, *519*, 4132-4135.
39. Y.-X. Liu, L.-F. Li, Y. Ning, Y.-Z. Lu, Q.-P. Lu, C.-M. Zhang, Y. Fang, A.-W. Tang, Y.-F. Hu, Z.-D. Lou, F. Teng and Y.-B. Hou. Effects of acetone-soaking treatment on the performance of polymer solar cells based on P3HT/PCBM bulk heterojunction. *Chinese Phys. B* **2014**, *23*, 118802.
40. W.J. Potscavage Jr., S. Yoo and B. Kippelen. Origin of the open-circuit voltage in multilayer heterojunction organic solar cells). *Appl. Phys. Lett.* **2008**, *93*, 193308.